PCCP

ROYAL SOCIETY OF CHEMISTRY

PAPER

View Article Online
View Journal | View Issue

Check for updates

Cite this: *Phys. Chem. Chem. Phys.*, 2023, **25**, 13198

Infrared photodissociation spectroscopy of mass-selected $[TaO_3(CO_2)_n]^+$ (n = 2–5) complexes in the gas phase†

Jia Han,‡[a] Yang Yang,‡[b] Binglin Qiu,‡[a] Pengcheng Liu,[a] Xiangkun Wu,[c] Guanjun Wang,*[b] Shilin Liu[a] and Xiaoguo Zhou*[a]

Received 27th March 2023,
Accepted 11th April 2023

DOI: 10.1039/d3cp01384g

rsc.li/pccp

We report a joint experimental and theoretical study on the structures of gas-phase $[TaO_3(CO_2)_n]^+$ (n = 2–5) ion–molecule complexes. Infrared photodissociation spectra of mass-selected $[TaO_3(CO_2)_n]^+$ complexes were recorded in the frequency region from 2200 to 2450 cm^{-1} and assigned through comparing with the simulated infrared spectra of energetically low-lying structures derived from quantum chemical calculations. With the increasing number of attached CO_2 molecules, the larger clusters show significantly enhanced fragmentation efficiency and a strong band appears at around 2350 cm^{-1} near the free CO_2 antisymmetric stretching vibration band, indicating only a small perturbation of CO_2 molecules on the secondary solvation sphere while higher frequency bands corresponding to the core structure remain largely unaffected. A core structure $[TaO_3(CO_2)_3]^+$ is identified to which subsequent CO_2 ligands are weakly attached and the most favorable cluster growth path is verified to proceed on the triplet potential energy surface higher in energy than that of ground states. Theoretical exploration reveals a two-state reactivity (TSR) scenario in which the energetically favored triplet transition state crosses over the singlet ground state to form a TaO_3^+ core ion, providing new information on the cluster formation correlated with the reactivity of tantalum metal oxides towards CO_2.

1. Introduction

Increases in emissions of anthropogenic carbon dioxide (CO_2) arising from fossil fuel use and tropical deforestation are responsible for global warming and worsening climatic situation.[1–3] Apart from natural sink and biological carbon pump counteracting the rapid growth of atmospheric CO_2 concentrations, achievement of industrial utilization of CO_2 as a renewable carbon source has been a subject of widespread public interest.[4,5] However, the biggest obstacle for speeding up the exploitation of chemical industry based on CO_2 as a raw material is its low energy level as well as chemical inertness, resulting from the highest oxidation state of carbon. Much emphasis has been placed on investigating CO_2 transformations and the related reaction mechanisms over the past two decades.[6–8]

The first crucial step in the conversion of CO_2 for further industrial applications refers to its activation by catalysts.[9] A promising approach to activate CO_2 is offered by its coordination to transition metal systems and detailed investigations of the fundamental interactions involved have been major subjects of extensive studies.[10–15] In this regard, gas-phase research in the absence of complicating effects, *i.e.* solvation, aggregation or surface inhomogeneities, is essential to elucidate binding motifs and activation process at a molecular level.[16] Infrared spectroscopy of mass-selected cluster ions where CO_2 ligates with a metal atom or metal oxide coupled with computational quantum chemistry plays a key role in unravelling intrinsic reaction mechanisms, energetics and kinetics.

Various binding modes of cationic metal–CO_2 complexes have been structurally summarized in the series of works reported by Duncan and coworkers, in which different clusters were formed during the complexation processes and could be characterized as follows: η^1-C, η^1-O, η^2-C,O and η^2-O,O coordination motifs.[17–21] Generally, a linear end-on M^+OCO

[a] *Hefei National Laboratory for Physical Sciences at the Microscale, Department of Chemical Physics, University of Science and Technology of China, Hefei, Anhui 230026, China. E-mail: xzhou@ustc.edu.cn*
[b] *Department of Chemistry, Collaborative Innovation Center of Chemistry for Energy Materials, Shanghai Key Laboratory of Molecular Catalysis and Innovative Materials, Fudan University, Shanghai, 200438, China. E-mail: gjwang@fudan.edu.cn*
[c] *Paul Scherrer Institute, 5232 Villigen, Switzerland*

† Electronic supplementary information (ESI) available: Optimized geometries of the $[TaO_3(CO_2)_n]^+$ (n = 2–5) complex isomers in the singlet and triplet states calculated at the PBE0-D3(BJ)/def2-TZVP level of theory (bond lengths in Ångströms and bond angles in degrees); relative energies of the $[TaO_3(CO_2)_n]^+$ (n = 2–5) complexes in the quintet state compared to those in singlet states (in kcal mol^{-1}). See DOI: https://doi.org/10.1039/d3cp01384g

‡ These authors contributed equally to this work.

structure would be expected from electrostatic considerations as the charge–quadrupole interaction typically dominates in the fundamental aspects of metal–CO_2 bonding. Moreover, Zhou and coworkers provided experimental evidence for the insertion reaction of metal cations into one C═O bond of carbon dioxide in $Ti^+(CO_2)_n$ metal–ion complexes.[22] A solvation-induced intracluster electron transfer reaction from metal to ligands has been observed in $V(CO_2)_n^+$ ($n \geq 7$) cluster ions, demonstrating the formation of an oxalate-type C_2O_4 anion species in large vanadium–CO_2 clusters.[23] In contrast to cationic species, notable CO_2 activations substantiated by significant red-shifts of CO_2 stretching vibrational frequency have been reported in the context of negatively charged $[M(CO_2)_n]^-$ cluster ions.[24–28]

Other promising candidates for catalytic applications such as transition metal oxides have been proposed recently, yet their reactions with CO_2 molecules are rarely explored compared to metal ions.[29–33] Observations of Fermi resonance of CO_2 in the inspection of interactions between free manganese oxide and CO_2 molecules indicated no evident contribution to CO_2 activation.[34] Studies on metal monoxide cations (ScO^+, YO^+, LaO^+ and HoO^+) with CO_2 using infrared photodissociation spectroscopy revealed that the conversion from solvated structures into carbonate motifs can be achieved by ScO^+, YO^+ and HoO^+ except for LaO^+.[32,35,36] Infrared spectra of gas-phase $NbO_2(CO_2)_n^+$ and $TaO_2(CO_2)_n^+$ complexes with rare-gas tagging showed leading solvation structures with the signature of a possible carbonate moiety in larger complexes.[37,38] In particular, TaO_2^+ has been proven to be more reactive in C–H bond activation of methane than the lighter congeners of VO_2^+ and NbO_2^+ in high-level theoretical calculations combined with mass spectrometric studies, resulting from the formation of a strong Ta–C bond.[39] Furthermore, thermal reactions investigated with mass spectrometry in conjunction with quantum chemical calculations conducted by the same group provided valuable insight into the role of TaO_3^+ in the activation of methane, which produced methanol and formaldehyde with concomitant release of methylene.[40] However, the large-scale reactivities of TaO_3^+ cations remain to be assessed.

Herein, we perform infrared photodissociation spectroscopy combined with quantum chemistry theoretical studies on $[TaO_3(CO_2)_n]^+$ (n = 2–5) ion–molecule complexes in the gas phase. The structures of complexes together with the salient features of intermolecular interactions between TaO_3^+ and CO_2 molecules are revealed based on the comparisons between the experimental spectra and simulated ones. This is the first investigation about CO_2 solvation around a transition metal trioxide cation to the best of our knowledge, shedding new light on the establishment of a suitable starting point to modify catalysts.

2. Experimental and computational methods

The infrared photodissociation spectra of mass-selected $[TaO_3(CO_2)_n]^+$ (n = 2–5) complexes were obtained using a collinear tandem time-of-flight (TOF) mass spectrometer coupled with a laser vaporization supersonic cluster source. The experimental instrument has been described in detail previously.[41,42] The 1064 nm fundamental of an Nd:YAG laser (Continuum, Minilite II; 10 Hz repetition rate and 6 ns pulse width) was used to vaporize a rotating tantalum metal target. The cation complexes were produced in the laser vaporization and expansion process of helium gas seeded with 2% CO_2 using a pulse valve (General Valve, Series 9) at the backing pressure of 1.0–1.2 $\times$ 10^6 Pa. After free expansion, the cations were skimmed and analyzed using a Wiley–McLaren TOF mass spectrometer. The ions of interest were mass-selected and decelerated into the extraction region of a second collinear TOF mass spectrometer where they were dissociated by a tunable IR laser. The fragment and parent ions were reaccelerated and mass-analyzed by the second TOF mass spectrometer. The ions were detected with a dual micro-channel plate (MCP) detector.

Infrared photodissociation spectra were recorded *via* monitoring the yield of the fragment ions as a function of dissociation IR laser wavelength and then normalizing to the parent ion signal. Typical spectra were recorded by scanning the dissociation laser in steps of 2 cm^{-1} and averaging over 300 laser shots at each wavelength. The tunable IR laser source was a KTP/KTA optical parametric oscillator/amplifier system (OPO/OPA, Laser Vision) pumped using a Continuum Powerlite 8000 Nd:YAG laser, and the output IR energy ranged from 1.0 to 2.0 mJ per pulse in the region of 2000–2500 cm^{-1}. The wavelength of the OPO laser was calibrated with a commercial wavemeter (Coherent, Wave-Master) using well-known CO absorptions. The IR beam path was purged with nitrogen to minimize air absorptions.

Quantum chemical calculations were performed to determine molecular structures and to validate vibrational assignments of the studied species. Considering that there might be various isomers at a specific mass-to-charge ratio, a large number of initial complex geometries were generated randomly by Genmer.[43,44] Preliminary screening was performed with the semiempirical quantum mechanical method GFN2-xTB,[45] using the xtb[46] program through Moclus.[43] The pre-optimized configurations were classified and sorted in energy. After extensive exploration, the resulting isomer ensembles (within 10 kcal mol^{-1}) were screened out for further optimization. The geometries of all minima and transition states were optimized using the PBE0-D3(BJ) functional in combination with the def2-TZVP basis set.[47,48] Harmonic vibrational frequencies were calculated at the same density functional level to verify that all of the minima have no imaginary frequencies, while the obtained transition states have one proper imaginary frequency. Intrinsic reaction coordinate (IRC) calculations were also performed to confirm that all of the reported transition states link the corresponding reactants and products.[49–52]

Notably, Ta^+, TaO^+ and TaO_2^+ cations have different spin ground electronic states,[37,53] *e.g.* quintet for Ta^+, triplet for TaO^+ and singlet for TaO_2^+, respectively. Likewise, the singlet, triplet and quintet spin states all probably exist for the TaO_3^+ cation, and hence all three spin states are necessary to be considered in vibrational assignments together with their

energetics. Based on computational results, all quintet $[TaO_3(CO_2)_n]^+$ complexes are significantly higher in energy than the singlet or triplet species and therefore excluded from further discussions (energetics are available in the ESI†). To theoretically predict IR spectra, harmonic vibrational frequencies were scaled by a factor of 0.957 and further convoluted with Lorentzian functions using 8 cm^{-1} full width at half-maximum (FWHM). This scaling factor was determined by comparing the experimental and calculated values of free CO_2 asymmetric stretching vibrational frequencies. All the DFT calculations were performed using the Gaussian 16 software package.[54]

3. Results and discussion

3.1 Mass spectrum and infrared photodissociation spectra of $[TaO_3(CO_2)_n]^+$ complexes

A typical TOF mass spectrum of cationic complexes produced by pulsed laser vaporization of a tantalum metal target in the expansion of CO_2/He mixture is shown in Fig. 1. Three progressions of mass peaks in the m/z range of 150–550 are clearly observed and identified to be CO_2 complexes of cationic tantalum oxides, *i.e.*, $[TaO_m(CO_2)_n]^+$ (m = 1–3) ion–molecule complexes. The dominant $[TaO_2(CO_2)_n]^+$ (n = 1–7) species were previously reported by Iskra and Mackenzie,[37] which is consistent with the high oxygen affinities of Ta^+ and TaO^+.[55] One noticeable difference between previous and our results is the formation of tantalum trioxide cation complexes $[TaO_3(CO_2)_n]^+$, albeit only a relatively small amount was detected. The tantalum trioxide cationic complexes $[TaO_3(CO_2)_n]^+$ had a maximum intensity at n = 2 in the mass spectrum while larger complexes with $n > 5$ were barely observed. Since $[TaO_2(CO_2)_n]^+$ (n = 1–7) species have been investigated previously,[37] in this work we paid more attention to larger ones, *i.e.* $[TaO_3(CO_2)_n]^+$ (n = 2–5), aiming to provide useful information for unravelling intermolecular interactions between TaO_3^+ and CO_2 ligands.

Given that the binding energy between TaO_3^+ and CO_2 for a small $[TaO_3(CO_2)_n]^+$ (n = 1) complex is greater than the infrared

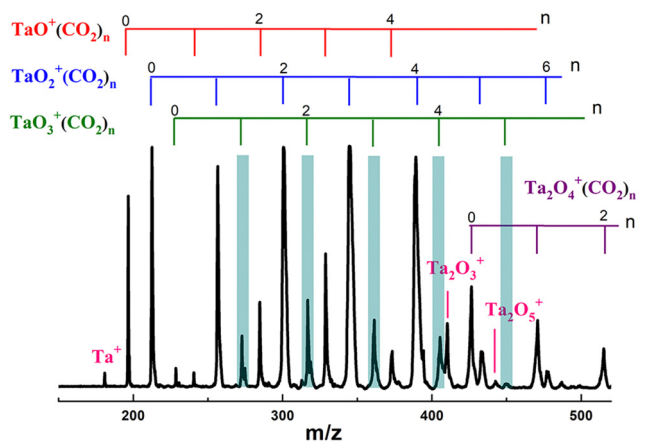

Fig. 1 Typical TOF mass spectrum produced by pulsed laser vaporization of a tantalum metal target in expansion of helium seeded with carbon dioxide.

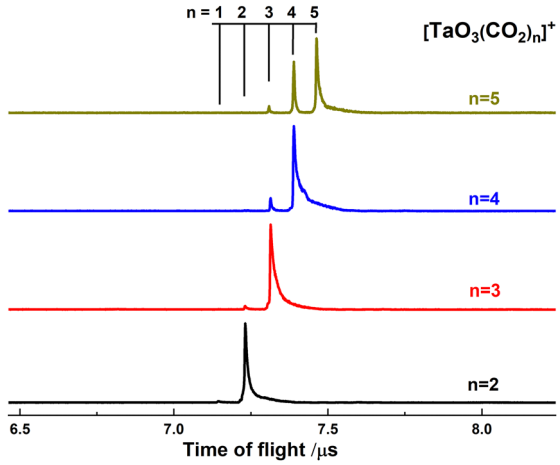

Fig. 2 The photodissociation action TOF mass spectra of $[TaO_3(CO_2)_n]^+$ (n = 2–5) ion–molecule complexes.

photon energy in the range of the CO_2 asymmetric stretching frequency, it is reasonable that we did not observe the photodissociation of $[TaO_3(CO_2)]^+$. For larger $[TaO_3(CO_2)_n]^+$ complexes with $n \geq 2$, their dissociation by losing one or more intact CO_2 ligands can occur under the action of IR laser (at 2360 cm^{-1}), as shown in Fig. 2. Apparently, only a small percentage of $[TaO_3(CO_2)_n]^+$ complexes for n = 2 and 3 dissociate, yet fragmentations of the larger clusters (n = 4 and 5) are more efficient. In particular, the loss of two CO_2 ligands was observed for the infrared dissociation of the $[TaO_3(CO_2)_5]^+$ complex.

By scanning infrared photon energy, the resulting infrared photodissociation spectra of $[TaO_3(CO_2)_n]^+$ (n = 2–5) complexes are shown in Fig. 3. The spectra for $[TaO_3(CO_2)_n]^+$ (n = 2 and 3) complexes have relatively poor signal-to-noise ratios, largely due to their inefficient dissociations. The cationic complexes

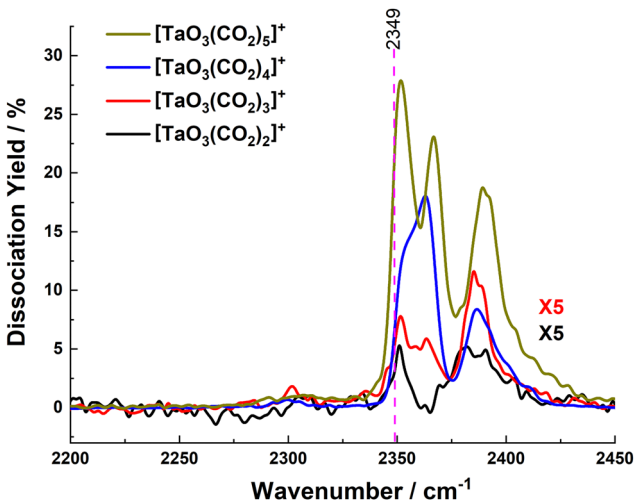

Fig. 3 Infrared photodissociation spectra of $[TaO_3(CO_2)_n]^+$ (n = 2–5) ion–molecule complexes in the photon energy range of 2200–2450 cm^{-1}, where the spectral intensities of $[TaO_3(CO_2)_2]^+$ and $[TaO_3(CO_2)_3]^+$ complexes are both amplified by a factor of 5 for comparison. The dashed line at 2349 cm^{-1} corresponds to the frequency of free CO_2 asymmetric stretching vibrational mode.

dissociate more efficiently with increasing cluster size.[56] All the evidence strongly implies that up to three CO_2 ligands can be tightly bound to the central TaO_3^+ core, analogous to the fully coordination number of 6 for the $[TaO_2(CO_2)_4]^+$ complex.[37] In other words, the fourth CO_2 molecule starts to form the second solvent shell, as the binding energy between the cationic core and the ligands on the second solvent shell is significantly lower in nature. In addition, only vibrational bands blue-shifted relative to that in isolated CO_2 are observed and no carbonyl stretching (2200–2250 cm^{-1}) is observed in Fig. 3, indicating that no insertion reaction occurs when TaO_3^+ interacts with CO_2 molecules, which is undoubtedly reasonable considering that the highest valence state of tantalum atom is +5.

3.2 Isomer identification and vibrational assignments of $[TaO_3(CO_2)_2]^+$

Among all $[TaO_3(CO_2)_n]^+$ (n = 2–5) complexes, $[TaO_3(CO_2)_2]^+$ is the most abundant species in the mass spectrum. Fig. 4 shows its experimental infrared spectrum in the frequency region of CO_2 antisymmetric stretching and the simulated IR spectra of two lowest-lying isomers each of singlet and triplet states, as well as their corresponding optimized geometries, spin states and relative energies (structural details are available in the ESI†). Two dominant absorptions consisting of a sharp peak at 2351 cm^{-1} and a wide band at around 2386 cm^{-1} are observed in the experimental spectrum. Nevertheless, all isomers of $[TaO_3(CO_2)_2]^+$ are found to exhibit two adjacent vibrational peaks in the CO_2 asymmetric stretching frequency range as shown in the simulated spectra. Therefore, more than one isomer should be formed in the current conditions according to complicated spectral features displayed in experiments.

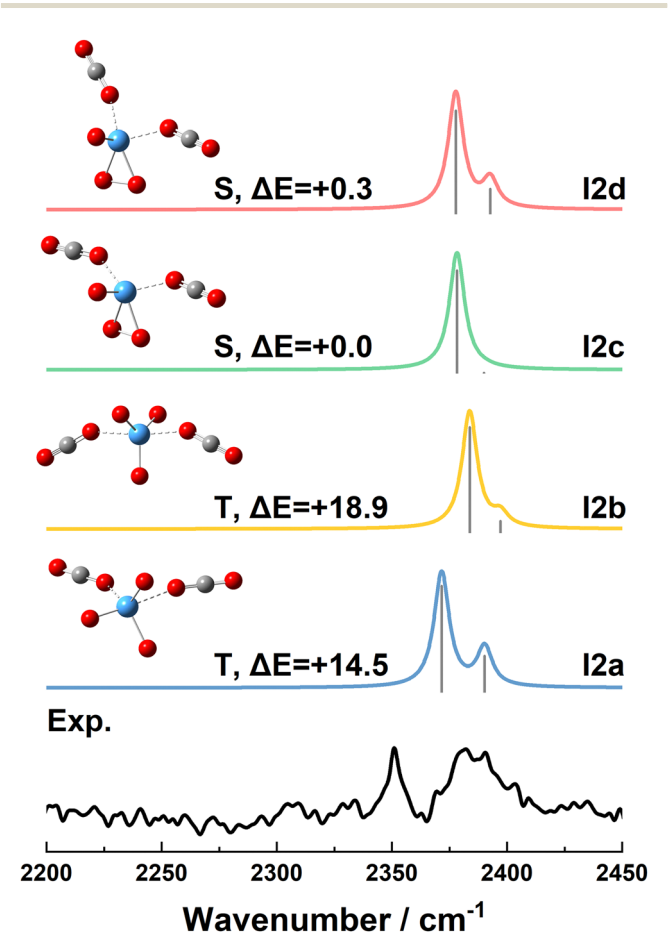

Fig. 4 Experimental and simulated vibrational spectra of the $[TaO_3(CO_2)_2]^+$ ion–molecule complex in the region of 2200–2450 cm^{-1}. The simulated spectra of isomers (**I2a–I2d**) were obtained from scaled theoretical harmonic frequencies and intensities for four low-lying structures in the singlet and triplet spin states at the PBE0-D3(BJ)/def2-TZVP level of theory. The corresponding spin states (S for singlet and T for triplet) and relative energies (in kcal mol^{-1}) of these isomers are noted as well.

The most stable isomer of $[TaO_3(CO_2)_2]^+$ complex **I2c** is in the singlet state with C_s planar symmetry. Due to the almost identical coordination modes between two CO_2 ligands and tantalum atoms, only one intense feature is predicted at 2378 cm^{-1} (panel of **I2c** in Fig. 4), consisting of the out-of-phase combination of asymmetric stretches of two CO_2 ligands. The second singlet isomer, **I2d**, higher in energy by 0.3 kcal mol^{-1} than **I2c**, involves a similar end-on coordination mode between the oxygen atom of the CO_2 ligand and the tantalum atom with a less symmetric bent structure. Both the in-phase and out-of-phase combinations of CO_2 asymmetric stretching motions are IR-active, giving rise to a two-peak structure covering the range of 2370–2395 cm^{-1} (panel of **I2d** in Fig. 4). On the triplet energy surface, the asymmetric energetically lowest-lying isomer, **I2a**, is higher in energy than the singlet minimum **I2c** by 14.5 kcal mol^{-1}. Two well-separated vibrations centered at 2372 and 2390 cm^{-1}, respectively, are clearly observed in the panel for the **I2a** isomer. In comparison to **I2d**, the relative intensities of these two peaks of **I2a** are closer. The second triplet isomer **I2b** lies 4.4 kcal mol^{-1} above **I2a**, featuring a main peak at 2383 cm^{-1} with a shoulder at 2397 cm^{-1} in the CO_2 antisymmetric stretching frequency region. Notably, only end-on coordination modes between tantalum atoms and CO_2 ligands are calculated in all these isomers, revealing the leading role of charge–quadrupole interactions in governing complex structures.

In view of direct spectral comparison, it is hard to conclusively assign the experimental spectrum of the $[TaO_3(CO_2)_2]^+$ complex to the absence of the theoretically predicted peak at 2351 cm^{-1} in all simulated spectra. However, all species discussed above still can be regarded as potential candidates in consideration of the overlap between the experimentally unresolved wide band on the higher-energy side and the spectral signatures of isomers in singlet or triplet states. From an energetic perspective, the wide band ranging from 2365 to 2406 cm^{-1} in the experimental spectrum should be attributed to the contribution of isomer **I2d** higher in energy by 0.3 kcal mol^{-1} than the global minimum **I2c**. Accordingly, **I2c** cannot be ruled out since the IR absorption calculated for **I2c** resides at nearly the same position with the main peak of **I2d**. In particular, the strong absorption of isomer **I2b** on the triplet surface provides the best match with the experimental feature of 2383 cm^{-1}, which is absent from the combined contribution of isomer **I2d** and **I2c**, clearly demonstrating the existence of

I2b under the present conditions. Moreover, it is reasonable that isomer **I2a** was populated in experiments as well considering that its energy is lower by 4.4 kcal mol^{-1} than **I2b** together with a similar band profile to the experimentally recorded spectrum. The spectral contribution of energetically high-lying triplet species may originate from their lower $TaO_3(CO_2)^+$–CO_2 binding energies compared to singlet isomers (see the ESI† for details). Additionally, the sharp peak at 2351 cm^{-1} in the experiment is very close to the vibrational frequency of free CO_2 asymmetric stretching (2349 cm^{-1}). Such a small frequency shift usually indicates that there is at least one CO_2 ligand bound by the weak interaction, yet isomers with characteristics of a weakly-bound CO_2 ligand have much higher energies regardless of singlet or triplet states in our calculations (not shown in Fig. 4). A probable explanation is that a few metastable states of $[TaO_3(CO_2)_2]^+$ with the $TaO_3(CO_2)^+\cdots CO_2$ structure may survive to be detected owing to the rapid free expansion. In fact, similar phenomena are not uncommon, for instance, Iskra *et al.*[11] observed the existence of a C_{2v} structure at around 0.21 eV above the global minimum for $Rh^+(CO_2)_2$–Ar complexes; and Thompson *et al.*[57] also found the main contribution from isomers with much higher energy in their discussion for small cluster sizes. Nevertheless, these metastable states naturally disappear with increasing cluster size during collisions with successive CO_2 molecules.

3.3 Isomer identification and vibrational assignments of $[TaO_3(CO_2)_3]^+$

The $[TaO_3(CO_2)_3]^+$ cation is the second abundant species among $[TaO_3(CO_2)_n]^+$ series in the mass spectrum. Its inefficient fragmentation as shown in Fig. 2 strongly implies that all three CO_2 ligands strongly bind to the core cation. Based on the optimized structures of three lowest-lying isomers of $[TaO_3(CO_2)_3]^+$ in singlet and triplet states, their simulated IR spectra are directly compared with the experimental results presented in Fig. 5. The experimental spectrum of the n = 3 complex exhibits a strong main feature together with a broader and weaker vibrational band close to the vibrational frequency of the free CO_2 asymmetric stretch. According to previously reported results,[35,37] the stronger one in the range of 2375–2410 cm^{-1} is attributed to the asymmetric stretching vibrations of monodentate coordinated CO_2 ligands. On the other hand, an unresolved wide band extending from 2345 to 2365 cm^{-1} reflects the formation of a weakly bound CO_2 ligand.

The most stable isomer **I3c** is located on the singlet state surface, and has C_s symmetry with three terminally bonded CO_2 ligands. Two peaks consist of three characteristic vibrations of **I3c** in the CO_2 asymmetrical stretching frequency region of 2360–2375 cm^{-1} (panel of **I3c** in Fig. 5). The lowest energy isomer in the triplet state (**I3a**) is calculated to be 20.3 kcal mol^{-1} higher than **I3c**, yet possessing almost the same structural motif as that the tantalum atom of TaO_3^+ center is coordinated by three terminal CO_2 units. Taking the analogous bonding patterns into consideration, it is not surprising that the calculated spectra of **I3a** and **I3c** are nearly identical to each other, each consisting of a main peak centered

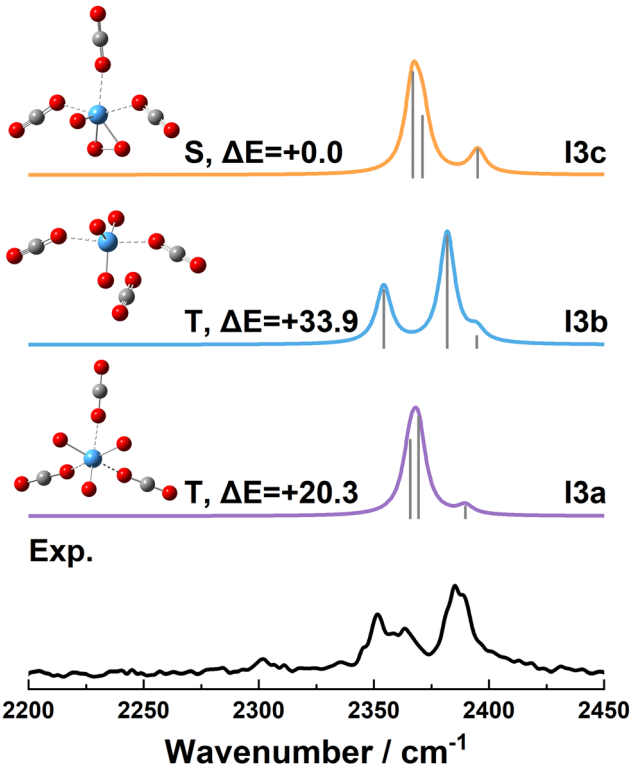

Fig. 5 Experimental and simulated vibrational spectra of the $[TaO_3(CO_2)_3]^+$ ion–molecule complex in the region of 2200–2450 cm^{-1}. The simulated spectra of isomers (**I3a–I3c**) were obtained from scaled theoretical harmonic frequencies and intensities for three low-lying structures in the singlet and triplet spin states at the PBE0-D3(BJ)/def2-TZVP level of theory. The corresponding spin states (S for singlet and T for triplet) and relative energies (in kcal mol^{-1}) of these isomers are noted as well.

at 2368 cm^{-1} and a weak band at around 2393 cm^{-1}. However, these calculated peak positions and relative intensities are far from the experimental observations. Therefore, these two isomers are disqualified as potential candidates for the experimental contributors. In addition, a third isomer **I3b** in the triplet state lies above **I3a** by 13.6 kcal mol^{-1}. Its structure involves two CO_2 ligands directly connected to the tantalum atom together with an exterior CO_2 molecule, which weakly binds to one of CO_2 ligand in the first coordination sphere (panel of **I3b** in Fig. 5). This structure can be viewed as derived from isomer **I2b** upon attaching a surface CO_2 molecule. The interpretation of two "inner" ligands and a weakly bound third ligand is borne out by calculated Ta–O bond lengths for the two "inner" ones of 2.17 Å, 2.21 Å and 3.32 Å for the third CO_2. The calculated spectrum of **I3b** exhibits a dominant peak at 2382 cm^{-1} with a shoulder at 2395 cm^{-1}, along with a relatively low-intensity peak centered at 2354 cm^{-1} arising from the weakly bound CO_2 molecule in the second solvation sphere. Notably, the strongest peak and its shoulder originated from the core ion $[TaO_3(CO_2)_2]^+$ coincide with the spectral signatures of isomer **I2b**.

Based on the best match with the experimental spectrum, the triplet isomer **I3b** can be regarded as the dominant contributor. However, it is unlikely that other low-lying isomers

like **I3a** are not populated in experiments. There are several clues for the presence of **I3a**. First, a weak peak at 2363 cm^{-1} is dimly visible in the low-frequency vibrational band (2345–2365 cm^{-1}) of the experimental spectrum, which is greatly consistent with the most prominent absorption in the calculated spectrum for **I3a**. Furthermore, considering that the binding energies between CO_2 ligands and the core structure in **I3a** are obviously greater than that in **I3b**, it is reasonable that IR photodissociation efficiency by monitoring the loss of one CO_2 molecule from **I3a** is naturally much smaller than that of **I3b**, leading to the observed vibrational features in experiments largely reproduced by isomer **I3b**. From an energy point of view, energetically high-lying isomer **I3b** is expected to be populated in a relatively small portion, in line with the overall low dissociation yield.

3.4 Isomer identification and vibrational assignments of $[TaO_3(CO_2)_4]^+$

As mentioned above, dissociation of $[TaO_3(CO_2)_4]^+$ *via* the loss of one CO_2 ligand is far more efficient than smaller complexes, implying a significantly lower binding energy for the fourth CO_2 molecule bound by weak electrostatic interactions. Fig. 6 shows the recorded IR photodissociation spectrum and the simulated vibrational spectra of five low-energy isomers predicted by DFT calculations. In the experimental spectrum, the most intense absorption featuring a doublet peak profile is located in a relatively low-frequency range of 2340–2370 cm^{-1}, while a weaker broad band is observed further to blue with a center at 2385 cm^{-1}. In particular, the existence of the shoulder at 2352 cm^{-1} strongly indicates that at least one CO_2 ligand is located on the second solvent shell.

The global minimum on the singlet spin surface, **I4d**, has C_s symmetry with four terminal bonded CO_2 ligands. Notably, it is an unconventional structure because the coordination number of the central tantalum atom exceeds its common maximal value of 6. As shown in the panel **I4d** in Fig. 6, all CO_2 ligands are directly bound to the core TaO_3^+ ion (Ta–O bond lengths of 2.26 and 2.31 Å, while the fourth CO_2 ligand is located somewhat further away with a Ta–O bond length of 2.47 Å), resulting in the deviation of all calculated vibrational frequencies of CO_2 antisymmetric stretch from that of isolated CO_2 molecule at 2349 cm^{-1}. In contrast to **I4d**, one CO_2 ligand in the second singlet isomer **I4e** starts to form the second solvent shell (Ta–O bond length of 3.69 Å), as shown in the panel of **I4e**. Although the binding interaction between this external CO_2 molecule and the cationic core is weaker than those of monodentate coordinated CO_2 ligands, the corresponding vibrational frequency is computed to be 2356 cm^{-1} and still higher to some extent than 2352 cm^{-1}. Therefore, both singlet isomers are excluded from dominant contributors to the experimental spectrum.

In contrast, no minimum for a four-coordinated $[TaO_3(CO_2)_4]^+$ complex could be found on the triplet potential energy surface. Instead, all starting four-coordinated structures converge into a central $[TaO_3(CO_2)_3]^+$ complex with a surface CO_2 molecule, where three CO_2 molecules complete the first coordination sphere around the TaO_3^+ core as isomer **I3a**. This coordination motif is consistent

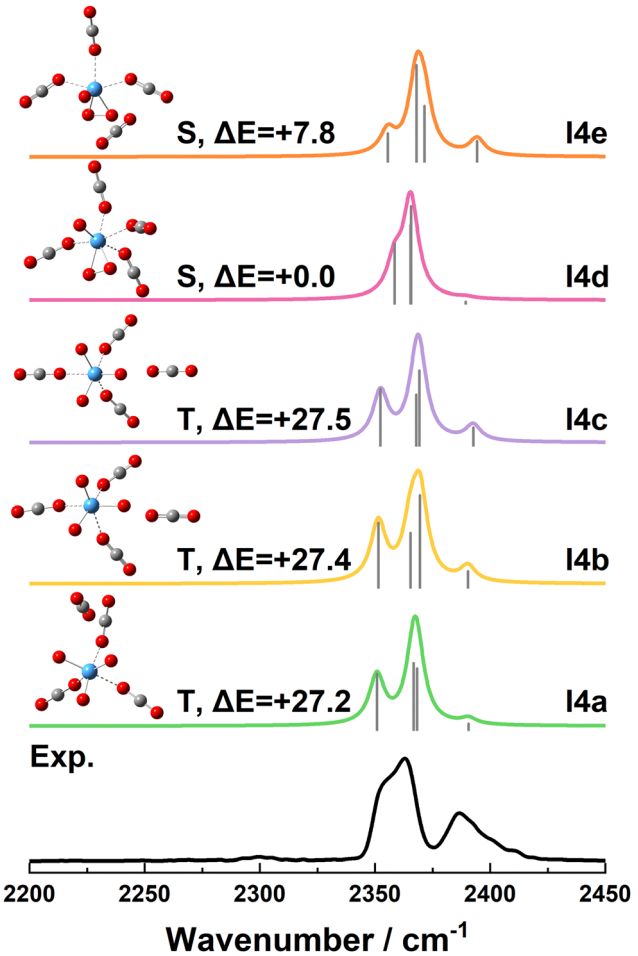

Fig. 6 Experimental and simulated vibrational spectra of the $[TaO_3(CO_2)_4]^+$ ion–molecule complex in the region of 2200–2450 cm^{-1}. The simulated spectra of isomers (**I4a–I4e**) were obtained from scaled theoretical harmonic frequencies and intensities for five low-lying structures in the singlet and triplet spin states at the PBE0-D3(BJ)/def2-TZVP level of theory. The corresponding spin states (S for singlet and T for triplet) and relative energies (in kcal mol^{-1}) of these isomers are noted as well.

with the significantly enhanced dissociation yields of $[TaO_3(CO_2)_n]^+$ complexes for $n > 3$. Therefore, we can expect that when one more CO_2 molecule is connected to the $[TaO_3(CO_2)_3]^+$ complex, the larger complex tends to preferentially saturate the inner shell layer regardless of whether the precursor is **I3b** or **I3a**. In other words, the three-coordinated structure of $[TaO_3(CO_2)_3]^+$ ion is essentially the core of larger complex ions. Consistently, all calculated low-lying structures of the $[TaO_3(CO_2)_4]^+$ complex comprise a three-coordinated core (a Ta–O bond length of ~2.3 Å) and an external CO_2 molecule with the Ta–O bond length larger than 3.0 Å. The binding energy of the fourth CO_2 ligand determined to be 5.8 kcal mol^{-1} is significantly lower than that of the third CO_2 (15.1 kcal mol^{-1}), reflecting the core structure as well. Due to weak perturbations, the addition of an extra CO_2 molecule has a negligible effect on the core structure and accordingly does not induce noticeable changes in the vibrational frequencies of tightly coordinated CO_2 ligands. Thus, it is plausible that the vibrational spectra of three triplet isomers, **I4a**, **I4b** and **I4c**, are nearly identical

to the calculated spectrum of **I3a** in the frequency range higher than 2360 cm^{-1}. Furthermore, their relative energies are also very close since the external CO_2 molecule is weakly attached to the oxygen atom of different inner CO_2 ligands. Apparently, this weak interaction accounts for the low-frequency vibrational frequency further to red. As shown in Fig. 6, newly arisen bands of these three isomers reside in virtually the same region at around 2352 cm^{-1} in the observed features.

Despite the fact that we failed to resolve the splitting of the first band ranging from 2340 to 2370 cm^{-1} under the conditions of our experiment, the positions and relative intensities of the simulated spectra for three lowest triplet isomers are all in good agreement with the experimental spectrum (Fig. 6). On the basis of the above analysis, we thus assign the experimental spectral features to the combined contributions from three low-lying triplet $[TaO_3(CO_2)_3–CO_2]^+$ structures.

3.5 Isomer identification and vibrational assignments of $[TaO_3(CO_2)_5]^+$

The $[TaO_3(CO_2)_5]^+$ cation shows low intensity in the mass spectrum yet is particularly susceptible to photodissociation in the energy region of CO_2 antisymmetric stretching vibrations. The larger complex is inclined to eliminate multiple CO_2 ligands, eventually terminating at the $n = 3$ species. Compared with other complex cations, the experimental spectrum of $[TaO_3(CO_2)_5]^+$ displays richer and clearer spectral features which is less challenging to interpret. Fig. 7 shows the experimental and simulated spectra of $[TaO_3(CO_2)_5]^+$ involving eight low-lying isomers in singlet or triplet states. In the experimental spectrum, three well-resolved bands are observed at 2352, 2367 and 2389 cm^{-1}, respectively, showing a decreasing trend of intensity with the increase of their frequencies. As the number of CO_2 ligands increases, the lowest-frequency vibrational band near the free CO_2 asymmetric stretching frequency (2349 cm^{-1}) shows stronger intensity, representing a conspicuous evolution of the spectra with cluster size.

For the $[TaO_3(CO_2)_5]^+$ complex on the singlet surface, a structure composed of a $[TaO_3(CO_2)_4]^+$ core ion and a fifth CO_2 loosely bound to the plane of symmetry (with the Ta–O bond length larger than 4.0 Å) is determined to be the global minimum (**I5e**). This isomer is likely to be formed by attaching one CO_2 molecule to the lowest-lying singlet $[TaO_3(CO_2)_4]^+$ complex, **I4d**. Although additional CO_2 molecule in the second coordination sphere contributes to the vibrational peak near 2349 cm^{-1}, the corresponding spectral intensity is relatively weak in comparison to the experimental data. Similar inconsistencies are also observed in the simulated spectra for other two low-lying singlet isomers, **I5f** and **I5g**, featuring an outer CO_2 weakly bound to the four-coordinated $[TaO_3(CO_2)_4]^+$ core. Therefore, these singlet isomers are all excluded from potential contributors to the experimental spectrum. Another low-lying singlet isomer **I5h** with C_s symmetry is higher in energy than **I5e** by 4.6 kcal mol^{-1}, offering an unusual coordination number of 5 for the TaO_3^+ core structure. However, the absence of any weakly-perturbed ligands rules out the presence of isomer **I5h** in this experiment.

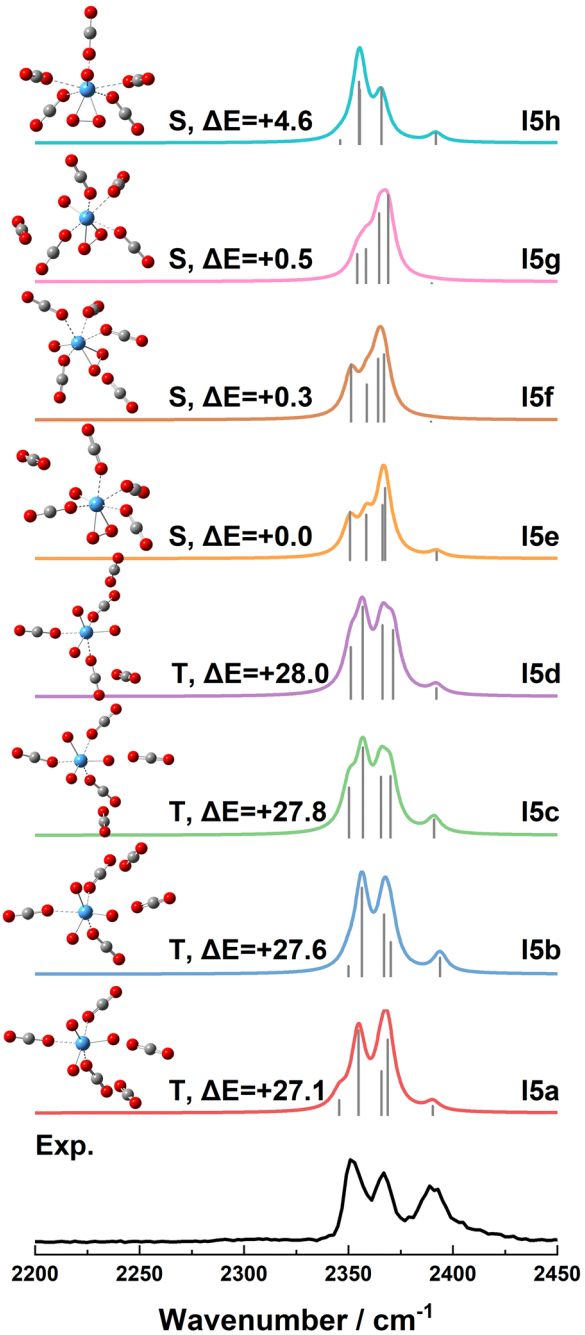

Fig. 7 Experimental and simulated vibrational spectra of the $[TaO_3(CO_2)_5]^+$ ion–molecule complex in the region of 2200–2450 cm^{-1}. The simulated spectra of isomers (**I5a–I5h**) were obtained from scaled theoretical harmonic frequencies and intensities for eight low-lying structures in the singlet and triplet spin states at the PBE0-D3(BJ)/def2-TZVP level of theory. The corresponding spin states (S for singlet and T for triplet) and relative energies (in kcal mol^{-1}) of these isomers are noted as well.

For the $[TaO_3(CO_2)_5]^+$ complex on the triplet potential energy surface, the coordination geometry of the core ion identified for all stable structures remains to be $[TaO_3(CO_2)_3]^+$ without exception. This arrangement can be thought of as evolving by successively attaching two more CO_2 ligands to the three-coordinated central metal oxide (with Ta–O bond lengths being

around 3.6 Å for outer ligands). While the variation of the location of weakly bound CO_2 molecules solvating the core ion has insignificant effects on the energetics, the simulated spectra show clear deviations with random solvation positions in spite of sharing a characteristic signature between 2340 and 2350 cm^{-1} which corresponds to the antisymmetric stretching vibrations of solvent CO_2 molecules. Exploratory computations reveal that the lowest energy site for the first external CO_2 molecule is near the CO_2 ligands bound in an end-on coordination fashion, whereas additional solvent molecules are determined to find their favorable solvation sites close to the oxygen atom of the metal oxide center. The distinct substructures of vibrational features appearing in the frequency region of 2340–2350 cm^{-1} can therefore be attributed to the differences in the configuration of the second solvation sphere. Moreover, there is little change in the spectral range correlated with three tightly bound CO_2 units, in accordance with the substantially identical core ion structures predicted by DFT calculations.

The simulated spectral patterns of isomer **I5c** together with **I5d**, which are higher in energy by 0.7 and 0.9 kcal mol^{-1} than the most stable isomer **I5a** in the triplet state, provide the best matches to the overall experimental spectra, demonstrating the presence of these geometries with a significant abundance in our experiment. Although there is insufficient information to confirm the existence of other triplet isomers, these structures are still likely to be populated in minority given the small energy window.

3.6 Implications of cluster growth

It is worth noting that the best matches for the experimental spectra consistently remain as clusters with triplet spin states instead of energetically lowest-lying singlet species. This is an unusual result from an energy perspective. Similar findings have been reported for the $VO_3(CO)_4^+$ cation with the high-lying triplet state accounting for experimental signatures.[58] In order to rationalize this intriguing reactivity promoted by the high-spin state, the key mechanistic aspects of core ion formation have been explored by means of theoretical calculations. Fig. 8 demonstrates the reaction profiles controlled by a two-state reactivity scenario involving both singlet and triplet spin states. On the potential energy surfaces of both states, the generation of the TaO_3^+ cation begins with the collision of TaO_2^+ and CO_2, forming an encounter complex with one oxygen atom of CO_2 approaching tantalum atom. Then an oxygen atom transfer reaction as the O atom shifts from the CO_2 molecule to the metal atom, leading to the $TaO_3^+\cdots CO$ transition state. This process involves the cleavage of a C═O bond and the formation of a new Ta–O bond. Since the ground electronic state of TaO_2^+ is singlet,[37,53] the entrance channel should locate on the singlet ground state which is lower in energy by 35.7 kcal mol^{-1} than the triplet state. However, it is impractical to overcome the extremely high energy barrier of 112.9 kcal mol^{-1} along the singlet pathway under current conditions. Notably, a spin crossover from the singlet to triplet *via* a cross point is much more favorable considering the significantly lower energy barrier through surmounting the triplet transition state as indicated in Fig. 8. Therefore, the triplet core ion TaO_3^+ could be

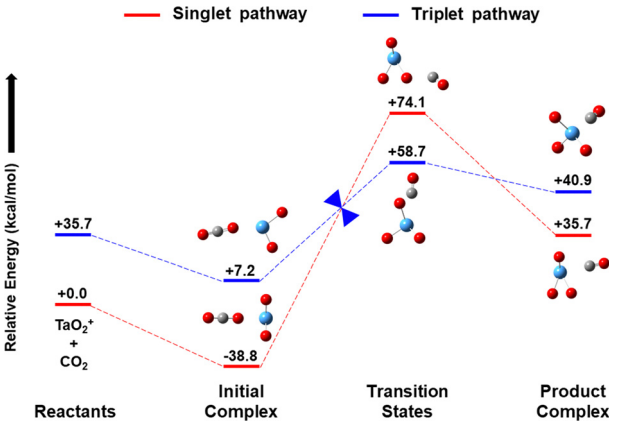

Fig. 8 Reaction pathways along potential energy surfaces for the formation of tantalum trioxide ion in the singlet and triplet spin states calculated at the PBE0-D3(BJ)/def2-TZVP level of theory, with relative energies in kcal mol^{-1}.

produced preferentially along the triplet reaction pathway as a result of a spin inversion from low to high spin state. This computationally determined reaction mechanism engaging a reaction surface that traverses two spin states perfectly explains the exclusive presence of triplet complexes in the experiments. Additionally, the formation of TaO_3^+ is endothermic either proceeding along singlet or triplet pathways, providing a reasonable explanation for relatively weak abundance of $[TaO_3(CO_2)_n]^+$ complexes in the mass spectrum (Fig. 1).

Based on the above analysis, an unconventional cluster growth of $[TaO_3(CO_2)_n]^+$ in the laser vaporization source is revealed to occur on the triplet energy landscape. Fig. 9 schematically presents two possible growth pathways by attaching successive CO_2 molecules to the TaO_3^+ cation starting with different initial isomers as **I2a** and **I2b**, respectively. With the addition of CO_2 molecules to the most stable isomer **I2a** in the triplet state, small clusters tend to stabilize through saturating the first coordination sphere, yielding a fully coordinated pattern with three tightly bound CO_2 units. Once the coordination of the core ion is completed, the subsequently preferable binding sites for successive ligands which experience weaker perturbation are in the proximity of the oxygen atoms of interior CO_2 units and central metal oxide. The geometry of the core ion somewhat distorts upon the attachment of further ligands with the Ta–O bond lengths for inner ligands remaining significantly shorter than those for the last two CO_2 molecules. In addition, the findings for the existence of high-lying isomer **I3b** with a relatively small population unveil an alternative way to grow, that is, the third CO_2 ligand is attached to the previously identified candidate structure **I2b**. This reaction pathway higher in energy accounts for a small percentage of cluster formation and terminates at $n = 3$, consistent with the signature of low fragmentation for experimental dissociation spectra for clusters of $n = 2$ and 3.

The differences between the fully coordinated core ion sizes for isomers **I2b** and **I3a** are associated with the geometric structures of the central metal oxide cation. For **I3a** with

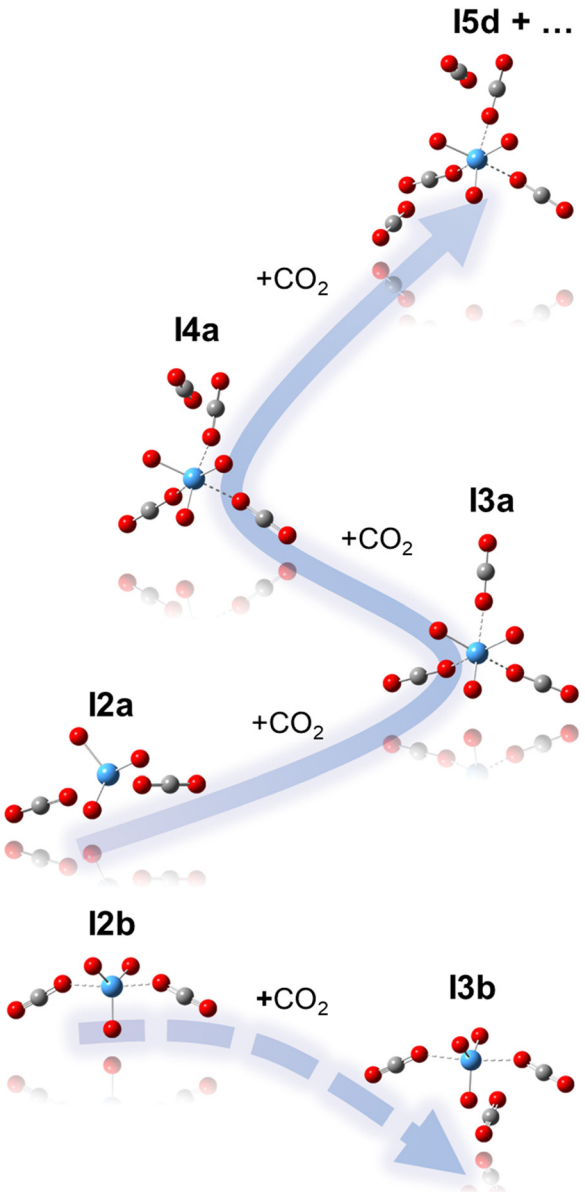

Fig. 9 Schematic illustration of cluster growth pathways for $[TaO_3(CO_2)_n]^+$ by successively attaching CO_2 molecules to the metal oxide center on the triplet potential energy surface.

pyramid oxide motifs, the compact core structure has three CO_2 ligands while **I3b** includes a solvent CO_2 molecule in the second coordination sphere around the core ion containing two CO_2 units. The change in the minimum core ion size corresponding to distinct metal oxide structures is a consequence of oxo ligands arranged in a planar configuration blocking coordination sites, therefore lowering the number of CO_2 ligands directly interacting with the metal atom.

4. Conclusions

Infrared photodissociation spectroscopy in conjunction with theoretical calculations is employed to investigate the structures of $[TaO_3(CO_2)_n]^+$ (n = 2–5) ion–molecule complexes in the gas phase. This work provides crucial insights into the cluster growth of CO_2 complexed around the tantalum trioxide cation as a model for CO_2 activation with metal oxide catalysts. Comparison of the experimental data with simulated spectra of low-lying isomers combined with photodissociation mass spectra allows for the identification of an energetically high-lying triplet $[TaO_3(CO_2)_3]^+$ core structure. A significant increase in the dissociation efficiency accompanied by observations of a strong vibrational band at wavenumbers close to the antisymmetric stretching frequency of the isolated CO_2 molecule for $n \geq 4$ complexes corroborates the presence of weakly bound CO_2 molecules in the second coordination sphere. The most intriguing finding in this structural study is the favorable cluster growth pathways along the triplet state rather than the seemingly accessible ground electronic state. A two-state reactivity involving spin crossing from the singlet to the triplet potential energy surface is revealed to be responsible for the experimental observation of the clusters in the triplet spin states which are less stable than corresponding singlet species. The reactivity of tantalum oxides and their interactions with CO_2 molecules remain an interesting topic to be investigated in future studies.

Author contributions

Jia Han: conceptualization, formal analysis, investigation, and writing – original draft; Yang Yang: investigation; Binglin Qiu: investigation; Pengcheng Liu: formal analysis; Xiangkun Wu: validation; Guanjun Wang: validation and methodology; Shilin Liu: funding acquisition and supervision; and Xiaoguo Zhou: funding acquisition and writing – review and editing.

Conflicts of interest

There are no conflicts of interest to declare.

Acknowledgements

This work was financially supported by the National Natural Science Foundation of China (no. 22073088, 21927805, 21903079 and 21873089) and the Ministry of Science and Technology of China (no. 2012YQ220113). The quantum chemical calculations were performed on the supercomputing system in the Supercomputing Center of the University of Science and Technology of China.

References

1 D. M. D'Alessandro, B. Smit and J. R. Long, Carbon Dioxide Capture: Prospects for New Materials, *Angew. Chem., Int. Ed.*, 2010, **49**, 6058–6082.
2 U. Siegenthaler and J. L. Sarmiento, Atmospheric Carbon Dioxide and the Ocean, *Nature*, 1993, **365**, 119–125.

3 S. Solomon, G.-K. Plattner, R. Knutti and P. Friedlingstein, Irreversible Climate Change Due to Carbon Dioxide Emissions, *Proc. Natl. Acad. Sci. U. S. A.*, 2009, **106**, 1704–1709.
4 T. Sakakura, J.-C. Choi and H. Yasuda, Transformation of Carbon Dioxide, *Chem. Rev.*, 2007, **107**, 2365–2387.
5 I. Omae, Aspects of Carbon Dioxide Utilization, *Catal. Today*, 2006, **115**, 33–52.
6 M. Mikkelsen, M. Jørgensen and F. C. Krebs, The Teraton Challenge. A Review of Fixation and Transformation of Carbon Dioxide, *Energy Environ. Sci.*, 2010, **3**, 43–81.
7 Y. Tsuji and T. Fujihara, Carbon Dioxide as a Carbon Source in Organic Transformation: Carbon–Carbon Bond Forming Reactions by Transition–Metal Catalysts, *Chem. Commun.*, 2012, **48**, 9956–9964.
8 V. Aomchad, À. Cristòfol, F. Della Monica, B. Limburg, V. D'Elia and A. W. Kleij, Recent Progress in the Catalytic Transformation of Carbon Dioxide into Biosourced Organic Carbonates, *Green Chem.*, 2021, **23**, 1077–1113.
9 B. M. Bhanage and M. Arai, *Transformation and Utilization of Carbon Dioxide*, Springer, 2014.
10 J. Zhuang, Z. H. Li, K. N. A. Fan and M. F. Zhou, Matrix Isolation Spectroscopic and Theoretical Study of Carbon Dioxide Activation by Titanium Oxide Molecules, *J. Phys. Chem. A*, 2012, **116**, 3388–3395.
11 A. Iskra, A. S. Gentleman, A. Kartouzian, M. J. Kent, A. P. Sharp and S. R. Mackenzie, Infrared Spectroscopy of Gas-Phase $M^+(CO_2)_n$ (M = Co, Rh, Ir) Ion–Molecule Complexes, *J. Phys. Chem. A*, 2017, **121**, 133–140.
12 S. D. Zhou, J. L. Li, M. Firouzbakht, M. Schlangen and H. Schwarz, Sequential Gas-Phase Activation of Carbon Dioxide and Methane by $[Re(CO)_2]^+$: The Sequence of Events Matters!, *J. Am. Chem. Soc.*, 2017, **139**, 6169–6176.
13 L. G. Dodson, M. C. Thompson and J. M. Weber, Characterization of Intermediate Oxidation States in CO_2 Activation, *Annu. Rev. Phys. Chem.*, 2018, **69**, 231–252.
14 D. Yang, X. T. Kong, H. J. Zheng, M. Z. Su, Z. Zhao, H. Xie, H. J. Fan, W. Q. Zhang and L. Jiang, Structures and Infrared Spectra of $[M(CO_2)_7]^+$ (M = V, Cr, and Mn) Complexes, *J. Phys. Chem. A*, 2019, **123**, 3703–3708.
15 Y. Yang, Y. K. Li, Y. X. Zhao, G. P. Wei, Y. Ren, K. R. Asmis and S. G. He, Catalytic Co-Conversion of CH_4 and CO_2 Mediated by Rhodium–Titanium Oxide Anions $RhTiO_2^-$, *Angew. Chem., Int. Ed.*, 2021, **60**, 13788–13792.
16 X. Cao, M. Chen, J. Ma, B. Yin and X. Xing, CO Oxidation by the Atomic Oxygen on Silver Clusters: Structurally Dependent Mechanisms Generating Free or Chemically Bonded CO_2, *Phys. Chem. Chem. Phys.*, 2017, **19**, 196–203.
17 A. M. Ricks, A. D. Brathwaite and M. A. Duncan, Coordination and Spin States in Vanadium Carbonyl Complexes $(V(CO)_n^+$, n = 1–7) Revealed with IR Spectroscopy, *J. Phys. Chem. A*, 2013, **117**, 1001–1010.
18 N. R. Walker, R. S. Walters and M. A. Duncan, Infrared Photodissociation Spectroscopy of $V^+(CO_2)_n$ and $V^+(CO_2)_nAr$ Complexes, *J. Chem. Phys.*, 2004, **120**, 10037–10045.
19 R. S. Walters, N. R. Brinkmann, H. F. Schaefer and M. A. Duncan, Infrared Photodissociation Spectroscopy of Mass-Selected $Al^+(CO_2)_n$ and $Al^+(CO_2)_nAr$ Clusters, *J. Phys. Chem. A*, 2003, **107**, 7396–7405.
20 G. Gregoire, N. R. Brinkmann, D. van Heijnsbergen, H. F. Schaefer and M. A. Duncan, Infrared Photodissociation Spectroscopy of $Mg^+(CO_2)_n$ and $Mg^+(CO_2)_nAr$ Clusters, *J. Phys. Chem. A*, 2003, **107**, 218–227.
21 G. Gregoire, J. Velasquez and M. A. Duncan, Infrared Photodissociation Spectroscopy of Small Fe^+–$(CO_2)_n$ and Fe^+–$(CO_2)_n$ Ar clusters, *Chem. Phys. Lett.*, 2001, **349**, 451–457.
22 X. P. Xing, G. J. Wang, C. X. Wang and M. F. Zhou, Infrared Photodissociation Spectroscopy of $Ti^+(CO_2)_2Ar$ and $Ti^+(CO_2)_n$ (n = 3–7) Complexes, *Chin. J. Chem. Phys.*, 2013, **26**, 687–693.
23 A. M. Ricks, A. D. Brathwaite, M. A. Duncan and I. R. Spectroscopy, of Gas Phase $V(CO_2)_n^+$ Clusters: Solvation-Induced Electron Transfer and Activation of CO_2, *J. Phys. Chem. A*, 2013, **117**, 11490–11498.
24 A. D. Boese, H. Schneider, A. N. Gloss and J. M. Weber, The Infrared Spectrum of $Au^-\cdot CO_2$, *J. Chem. Phys.*, 2005, **122**, 154301.
25 B. J. Knurr and J. M. Weber, Solvent-Driven Reductive Activation of Carbon Dioxide by Gold Anions, *J. Am. Chem. Soc.*, 2012, **134**, 18804–18808.
26 B. J. Knurr and J. M. Weber, Solvent-Mediated Reduction of Carbon Dioxide in Anionic Complexes with Silver Atoms, *J. Phys. Chem. A*, 2013, **117**, 10764–10771.
27 B. J. Knurr and J. M. Weber, Infrared Spectra and Structures of Anionic Complexes of Cobalt with Carbon Dioxide Ligands, *J. Phys. Chem. A*, 2014, **118**, 4056–4062.
28 B. J. Knurr and J. M. Weber, Interaction of Nickel with Carbon Dioxide in $[Ni(CO_2)_n]^-$ Clusters Studied by Infrared Spectroscopy, *J. Phys. Chem. A*, 2014, **118**, 8753–8757.
29 M. K. Koh, Y. J. Wong, S. P. Chai and A. R. Mohamed, Carbon Dioxide Hydrogenation to Methanol Over Multi-Functional Catalyst: Effects of Reactants Adsorption and Metal-Oxide(s) Interfacial Area, *J. Ind. Eng. Chem.*, 2018, **62**, 156–165.
30 G. Y. Liu, T. P. Thanh, H. J. Chen and A. Tricoli, A Review of Metal- and Metal-Oxide-Based Heterogeneous Catalysts for Electroreduction of Carbon Dioxide, *Adv. Sustainable Syst.*, 2018, **2**, 1800028.
31 X. L. Liu, M. H. Wang, H. R. Yin, J. T. Hu, K. Cheng, J. C. Kang, Q. H. Zhang and Y. Wang, Tandem Catalysis for Hydrogenation of CO and CO_2 to Lower Olefins with Bifunctional Catalysts Composed of Spinel Oxide and SAPO-34, *ACS Catal.*, 2020, **10**, 8303–8314.
32 E. I. Brewer, A. E. Green, A. S. Gentleman, P. W. Beardsmore, P. A. J. Pearcy, G. Meizyte, J. Pickering and S. R. Mackenzie, An Infrared Study of CO_2 Activation by Holmium Ions, Ho^+ and HoO^+, *Phys. Chem. Chem. Phys.*, 2022, **24**, 22716–22723.
33 L. G. Dodson, M. C. Thompson and J. M. Weber, Interactions of Molecular Titanium Oxides TiO_x (x = 1–3) with Carbon Dioxide in Cluster Anions, *J. Phys. Chem. A*, 2018, **122**, 6909–6917.
34 N. Zimmermann, T. M. Bernhardt, J. M. Bakker, R. N. Barnett, U. Landman and S. M. Lang, Infrared Spectroscopy

of Gas-Phase $Mn_xO_y(CO_2)_z^+$ Complexes, *J. Phys. Chem. A*, 2020, **124**, 1561–1566.
35 D. Yang, M. Z. Su, H. J. Zheng, Z. Zhao, X. T. Kong, G. Li, H. Xie, W. Q. Zhang, H. J. Fan and L. Jiang, Infrared Spectroscopy of CO_2 Transformation by Group III Metal Monoxide Cations, *Chin. J. Chem. Phys.*, 2020, **33**, 160–166.
36 Z. Zhao, X. T. Kong, Q. Q. Yuan, H. Xie, D. Yang, J. J. Zhao, H. J. Fan and L. Jiang, Coordination-Induced CO_2 Fixation into Carbonate by Metal Oxides, *Phys. Chem. Chem. Phys.*, 2018, **20**, 19314–19320.
37 A. Iskra, A. S. Gentleman, E. M. Cunningham and S. R. Mackenzie, Carbon Dioxide Binding to Metal Oxides: Infrared Spectroscopy of $NbO_2^+(CO_2)_n$ and $TaO_2^+(CO_2)_n$ Complexes, *Int. J. Mass Spectrom.*, 2019, **435**, 93–100.
38 X. T. Kong, R. L. Shi, C. Wang, H. J. Zheng, T. T. Wang, X. Q. Liang, J. P. Yang, Q. S. Jing, Y. M. Liu and H. Y. Han, *et al.*, Interaction between CO_2 and NbO_2^+: Infrared Photodissociation Spectroscopic and Theoretical Study, *Chem. Phys.*, 2020, **534**, 110755.
39 S. Zhou, J. Li, M. Schlangen and H. Schwarz, Differences and Commonalities in the Gas-Phase Reactions of Closed–Shell Metal Dioxide Clusters $[MO_2]^+$ (M = V, Nb, and Ta) with Methane, *Chem. – Eur. J.*, 2016, **22**, 7225–7228.
40 S. D. Zhou, J. L. Li, M. Schlangen and H. Schwarz, Spin-Selective Thermal Activation of Methane by Closed–Shell $[TaO_3]^+$, *Angew. Chem., Int. Ed.*, 2016, **55**, 7257–7260.
41 G. J. Wang, C. X. Chi, J. M. Cui, X. P. Xing and M. F. Zhou, Infrared Photodissociation Spectroscopy of Mononuclear Iron Carbonyl Anions, *J. Phys. Chem. A*, 2012, **116**, 2484–2489.
42 G. J. Wang, C. X. Chi, X. P. Xing, C. F. Ding and M. F. Zhou, A Collinear Tandem Time-of-Flight Mass Spectrometer for Infrared Photodissociation Spectroscopy of Mass-Selected Ions, *Sci. China: Chem.*, 2014, **57**, 172–177.
43 T. Lu, *Molclus Program, 1.9.9.3*, **https://www.keinsci.com/research/molclus.html**, 2021 (accessed July 8 2021).
44 T. Lu and F. W. Chen, Multiwfn: A Multifunctional Wavefunction Analyzer, *J. Comput. Chem.*, 2012, **33**, 580–592.
45 C. Bannwarth, S. Ehlert and S. Grimme, GFN2-xTB-An Accurate and Broadly Parametrized Self-Consistent Tight-Binding Quantum Chemical Method with Multipole Electrostatics and Density-Dependent Dispersion Contributions, *J. Chem. Theory Comput.*, 2019, **15**, 1652–1671.
46 S. Grimme, C. Bannwarth and P. Shushkov, A Robust and Accurate Tight-Binding Quantum Chemical Method for Structures, Vibrational Frequencies, and Noncovalent Interactions of Large Molecular Systems Parametrized for All spd-Block Elements (Z = 1–86), *J. Chem. Theory Comput.*, 2017, **13**, 1989–2009.
47 C. Adamo and V. Barone, Toward Reliable Density Functional Methods without Adjustable Parameters: The PBE0 model, *J. Chem. Phys.*, 1999, **110**, 6158–6170.
48 S. Grimme, S. Ehrlich and L. Goerigk, Effect of the Damping Function in Dispersion Corrected Density Functional Theory, *J. Comput. Chem.*, 2011, **32**, 1456–1465.
49 K. Fukui, Formulation of the Reaction Coordinate, *J. Phys. Chem.*, 1970, **74**, 4161–4163.
50 K. Fukui, The Path of Chemical Reactions-The IRC Approach, *Acc. Chem. Res.*, 1981, **14**, 363–368.
51 C. Gonzalez and H. B. Schlegel, Reaction Path Following in Mass-Weighted Internal Coordinates, *J. Phys. Chem.*, 1990, **94**, 5523–5527.
52 D. G. Truhlar and M. S. Gordon, From Force Fields to Dynamics: Classical and Quantal Paths, *Science*, 1990, **249**, 491–498.
53 M. F. Zhou and L. Andrews, Reactions of Laser-Ablated Niobium and Tantalum Atoms with Oxygen Molecules: Infrared Spectra of Niobium and Tantalum Oxide Molecules, Anions, and Cations, *J. Phys. Chem. A*, 1998, **102**, 8251–8260.
54 M. J. Frisch; G. W. Trucks; H. B. Schlegel; G. E. Scuseria; M. A. Robb; J. R. Cheeseman; G. Scalmani; V. Barone; G. A. Petersson and H. Nakatsuji, *et al.*, *Gaussian 16, Rev. C.01*, Gaussian, Inc., Wallingford, CT, 2016.
55 R. Wesendrup and H. Schwarz, Tantalum-Mediated Coupling of Methane and Carbon-Dioxide in the Gas-Phase, *Angew. Chem., Int. Ed. Engl.*, 1995, **34**, 2033–2035.
56 A. M. Ricks, Z. D. Reed and M. A. Duncan, Seven-Coordinate Homoleptic Metal Carbonyls in the Gas Phase, *J. Am. Chem. Soc.*, 2009, **131**, 9176–9177.
57 M. C. Thompson and J. M. Weber, Infrared Photodissociation Spectra of $[Sn(CO_2)_n]^-$ Cluster Ions, *J. Phys. Chem. A*, 2018, **122**, 3772–3779.
58 A. D. Brathwaite, A. M. Ricks and M. A. Duncan, Infrared Photodissociation Spectroscopy of Vanadium Oxide–Carbonyl Cations, *J. Phys. Chem. A*, 2013, **117**, 13435–13442.

